Polym. Bull. (2012) 68:1469–1482
DOI 10.1007/s00289-011-0689-3

ORIGINAL PAPER

Effect of silica nanoparticles on structure and properties of waterborne UV-curable polyurethane nanocomposites

Shengwen Zhang · Aixia Yu · Shilin Liu · Jie Zhao · Jinqiang Jiang · Xiaoya Liu

Received: 9 October 2011 / Revised: 2 November 2011 / Accepted: 6 December 2011 /
Published online: 18 December 2011

Abstract UV-curable waterborne polyurethane (WUPU)/silica nanocomposites were prepared using various silica by phase-inversion emulsification method. TEM examinations of nanostructured films indicated that the organic modified nanosilica was well dispersed in the WUPU matrix, while the acid and alkaline silica formed much less compact, or densely aggregated structure. DMA analysis demonstrated that the WUPU/silica nanocomposite films had a broadening of the tanδ peak and shifted to higher temperature. The WUPU/silica nanocomposite films displayed enhanced storage modulus, Shore A hardness, tensile strength without sacrificing high elongation at break compared to that of the pure WUPU film. The resulting nanocomposite films are possibly interesting for the generation of waterborne UV-curable transparent coatings with scratch-resistance.

Keywords UV-curable · Waterborne polyurethane · Silica · Nanocomposites

Introduction

Polyurethane dispersions (PUD) and especially UV-curing polyurethane dispersions (UV-PUD) have been increasingly used in many industrial applications such as coatings, adhesives and inks because of their zero/low volatile organic compounds (VOCs), excellent film forming properties and versatile performance properties [1, 2]. Their films show an excellent elasticity and toughness. But the mechanical strength and stiffness of these films are typically inferior to conventional solvent borne PU films. Inorganic filler are commonly used in waterborne polyurethane (WPU) to reinforce the WPU films. But the improvements in modulus for WPU

S. Zhang (✉) · A. Yu · S. Liu · J. Zhao · J. Jiang · X. Liu
School of Chemical & Material Engineering, Jiang Nan University, Wu Xi 214122,
People's Republic of China
e-mail: zsw0825@Yahoo.com

composites are at the expense of substantially reduced elongation at break. Incorporation of the nanosized fillers into a WPU matrix is an effective strategy to enhance the properties of WPU films. Various WPU nanocomposites such as silica [3–8], clay [9–12], carbon nanotube [13–15], cellulose nanocrystals [16, 17], polyhedral oligomeric silsesquioxanes (POSS) [18, 19], ZnO [20] were reported to exhibit the unusual combination of increased tensile strength and Young's modulus without sacrificing high elongation at break.

As compared to other inorganic nanofillers, silica nanoparticles have many advantages, including high hardness and relatively low refractive index, commercially availability of a wide range of relatively cheap ultrafine silica particles: aqueous silica sol, precipitated or fumed silica, nanosilica generated by sol–gel method. In addition, silica has silanol group on the surface, which can form hydrogen-bonding interaction with the hard and/or soft segments of polyurethane [21]. So nanosilica is expected to offer attractive potential in WPU reinforcement. Considerable efforts have been concentrated on the refinement of processing techniques (including colloidal-physics method [3, 15, 20], in situ polymerization method [9, 18]), and nanosilica surface functionalization[4, 5, 8], silanized polyurethane [6], and generated nanosilica in situ by sol–gel method [7] to control the well dispersion of nanosilica in WPU matrix. However, achieving the homogeneous distribution of silica nanoparticles in WPU films with cost-effective method is still a challenging problem. Recently, we have developed a facile method to prepare waterborne UV-curable polyurethane/silica nanocomposites by phase-inversion emulsification method [22]. It was found that the silica nanoparticles were well dispersed in the WUPU matrix. However, the obtained results have further demonstrated that the correlation of morphology of the nanocomposite with the macroscopic performance is needed to study. In this article, the effect of silica surface chemistry and particles size on the microstructure and properties of WUPU/silica nanocomposites were evaluated.

Experimental

Materials

Polyethylene Glycol (PEG, $M_n = 400$) was distilled before use. Dimethylol propionic acid (DMPA) was dried at 80 °C for 24 h in a vacuum oven. Hydroxyethyl methacrylate (HEMA) was distilled before use. Acetone was dried over 4 Å molecular sieves before use. Isophorone diisocyanate (IPDI), triethylamine (TEA), Dibutyltin dilaurate (DBTDL), Hydroquinone, 2-hydroxy-1-4-[(2-hydroxyethoxy)-phenyl]-2-methyl-1-propanone (the photoinitiator Irgacure 2959, Ciba Specialty Chemicals) were used as received. Aqueous colloidal silica (R301, 30 wt% silica, average diameter 10 nm, pH 10.5; R900, 34 wt% silica, diameter 20 nm, pH 3.0) was obtained from Akzo Nobel. W75, the aqueous dispersions of fumed silica, pH 4.5, average diameter 132 nm, 30 wt% silica (Degussa), Tetraethyl orthosilicate, absolute ethanol, ammonium hydroxide, and toluene (Shanghai Chemistry Reagent Co.) and methacryloxy (propyl) trimethoxysilane (MEMO) (Degussa) were used as received.

The Silica-MEMO was synthesized according to our previous method [23]. Its average diameter was 95 nm.

Preparation of WUPU/silica nanocomposite dispersions

The WUPU/silica nanocomposite dispersions were prepared according to the following procedure. In a 250 mL round-bottom four-necked flask with a mechanical stirrer, thermometer, condenser and nitrogen in/outlet, 24.5 g IPDI was charged into the dried flask. 31.5 g PEG 400 and four drops of DBTDL were added dropwise and reacted at 45 °C for 1–2 h. The isocyanate (NCO) content was monitored during the reaction using the standard dibutylamine back-titration method. Upon reaching the theoretical NCO value, 2.85 g hydrophilic monomer (DMPA) and two drops of DBTDL were added and reacted at 60 °C until the NCO content reached another theoretical value. Subsequently 2.6 g HEMA and 0.06 g of the inhibitor hydroquinone were added to react at 70 °C for 3–4 h. The reaction end point was confirmed by the disappearance of the IR absorption peak at 2270 cm^{-1} corresponding to stretching vibration of the NCO group. During the above process, acetone was added to adjust the viscosity of the PU prepolymers and its solid content was about 65–75 wt%. For neutralizing the resulting PU prepolymers, 2.15 g TEA was added and stirred for 1 h at 50 °C. Then the aqueous silica sol was added and stirred for 1 h at 50 °C (10 wt% based on the WUPU resins). Formation of the WUPU/silica nanocomposite was accomplished by slowly adding the water to the neutralized acetone solution of the PU prepolymers at ambient temperature with an agitation speed of 600 rpm. The above dispersion was transferred to a rotary evaporator, and the acetone was removed to afford WUPU/silica nanocomposite dispersions with 15 wt% solid content and pH value of 7.0–8.0.

To this, 3–4 wt% of photoinitiator (Irgacure 2959) was added and dispersed in the WUPU/silica dispersions with the aid of ultrasound. Then, the films were prepared by casting the dispersion onto Teflon mold, followed by slowly drying at 45 °C for 24 h. The resulting films were then heated in an oven at 60 °C for 0.5 h. Films were irradiated from one side using 200 W UV (365 nm) lamp for 2 min at room temperature. The films obtained were cut for the mechanical measurements.

Table 1 Glass transition temperatures and cross-link density of WUPU/silica nanocomposite films

Sample	T_g(°C)	E' (MPa) (T = 80 °C)	Cross-link density ($\times 10^2$ mol m^{-3})	Gel content (%)	Swell ratio
WUPU	T_g-S = 9.2, T_g-H = 52.8	0.42	0.51	95	1.36
WUPU/R900	T_g-S = 17.8	1.96	2.36	93	1.37
WUPU/ silica-MEMO	T_g-S = 14.6	0.95	1.14	94	1.38
WUPU/R301	T_g-S = 11.5	0.62	0.75	91	1.40
WUPU/W75	T_g-S = 17.8	0.62	0.75	88	1.45

Methods

A Fourier transform infrared spectrophotometer (FTLA2000-104, ABB Bomem of Canada) was used to identify the chemical structure of PUA prepolymers. For transmission electron microscopy (TEM), the nanocomposite film was embedded in a resin. The embedded specimen was sectioned with a Leica Ultracut-E using a glass knife. The sections of approximately 100 nm thickness were mounted on a grid with carbon support. The section was then examined with a JEOL-1010 apparatus. The morphology in the cross section of films was examined on the scanning electron microscope (SEM, S4800, Hitachi). The nanocomposite films were fractured in liquid nitrogen and gold-sputtered prior to SEM imaging. Dynamic mechanical thermal analysis (DMTA) of the nanocomposite films was carried out using a TA Instruments DMA 2980 dynamic mechanical analyzer in the tensile mode. The viscoelastic properties of the nanocomposite films were measured under a nitrogen atmosphere, at a heating rate of 2 °C/min from −80 to 150 °C and a frequency of 1 Hz. The mechanical properties such as tensile strength and elongation at break were investigated by the LRX Plus equipment. The samples were cut into dumbbell shapes and the tensile stress–strain measurements were obtained from the films. The cross-head speed was set at 50 mm/min, and the test continued until sample failure. A minimum of three tests were analyzed for each sample, and the average values are reported. Shore A hardness was measured using an indentation hardness tester according to ASTM D2240-75. The transmittance of the prepared nanocomposite films (ca. 0.5 mm thickness) was measured by using the UV–vis spectrophotometer (Perkin-Elmer, Lambda 25). Thermogravimetric analysis (TGA) was performed on a TGA/1/1100 SF (Mettler Toledo) instrument. The samples were heated from room temperature to 800 °C at a heating rate of 20 °C/min in N_2 atmosphere (flow rate of 50 mL/min).

Results and discussion

Nanosilica dispersion and morphology

The state of dispersion of inorganic nanoparticles in a polymer matrix can vary from highly dispersed to totally aggregated, depending on both particle–particle and polymer segment-particle surface interactions [24, 25]. It was reported that the unfunctionalized silica particles tended to agglomerate into large spherical structures with diameters in the range 1–100 μm to minimize the contact area between the silica particle and the hydrophobic polymer phase [26] and the bare silica particles could also be well dispersed in PMMA [27] and acrylated HBP polymer matrix [28] through strong hydrogen-bonding interactions. Figure 1 shows TEM images of thin sections of the cured WUPU/silica nanocomposite films. For R301, The small aggregates presented in the electron micrographs consist of approximately 2–3 loosely associated individual particles (Fig. 1a). These aggregates had mutual contact and occupied the most regions of the WUPU matrix. The certain miscibility between the hydrophilic nature of PEG soft segment of WUPU

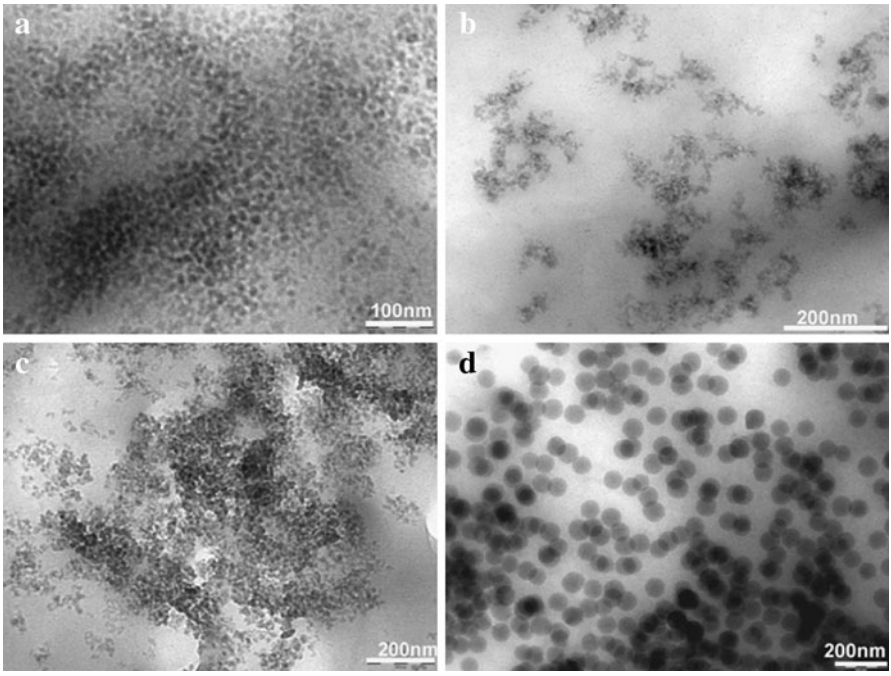

Fig. 1 TEM diagrams of the WUPU/silica nanocomposite films: **a** WUPU-R-301, **b** WUPU-R900, **c** WUPU-W75, **d** WUPU-MEMO

and hydrophilic silica particles is helpful for the R301 dispersion in WUPU matrix. The R301 did not agglomerate into large spherical structures or isolated particles and formed loosely interconnected structure, which indicates that the hydrogen-bonding interaction dominantly takes place between the silica particles and to a lesser extent between the silanol group and the urethane groups in the HS domains. Evidence for this fact is seen in SEM image of the nanocomposite fracture surfaces (Fig. 2a) where we showed that evident nanosilica clusters pull-out and extensive interface delamination during fracture. In contrast, for the R900, a significant amount of aggregation also occurred with structures in the range of 100–500 nm in diameter (Fig. 1b). These aggregates had no mutual contact and much less compact and were surrounded by large areas of WUPU matrix. The fracture surfaces that were flatter and only some small silica clusters are discernible on the fractured surfaces of the specimens (see Fig. 2b), because the silica surface was covered by a layer of WUPU polymer. We ascribed it to the ionic interactions between the COO^{-} ions hard segments of WPU and cationic silica particles. For R900 is an acid silica sol with cationic particles stabilized by chloride. But for an acid W75, a fractal type of aggregation and an overlapping of the aggregates are observed (Fig. 1c). The fracture surfaces also contained numerous dense silica aggregates (Fig. 2c). It is mainly related to the surface nature of the W75. It is the dispersions of fumed silica with the intensity average size about 132 nm and not like R900 stabilized by chloride, which limits its interaction with WUPU. For the MEMO modified silica,

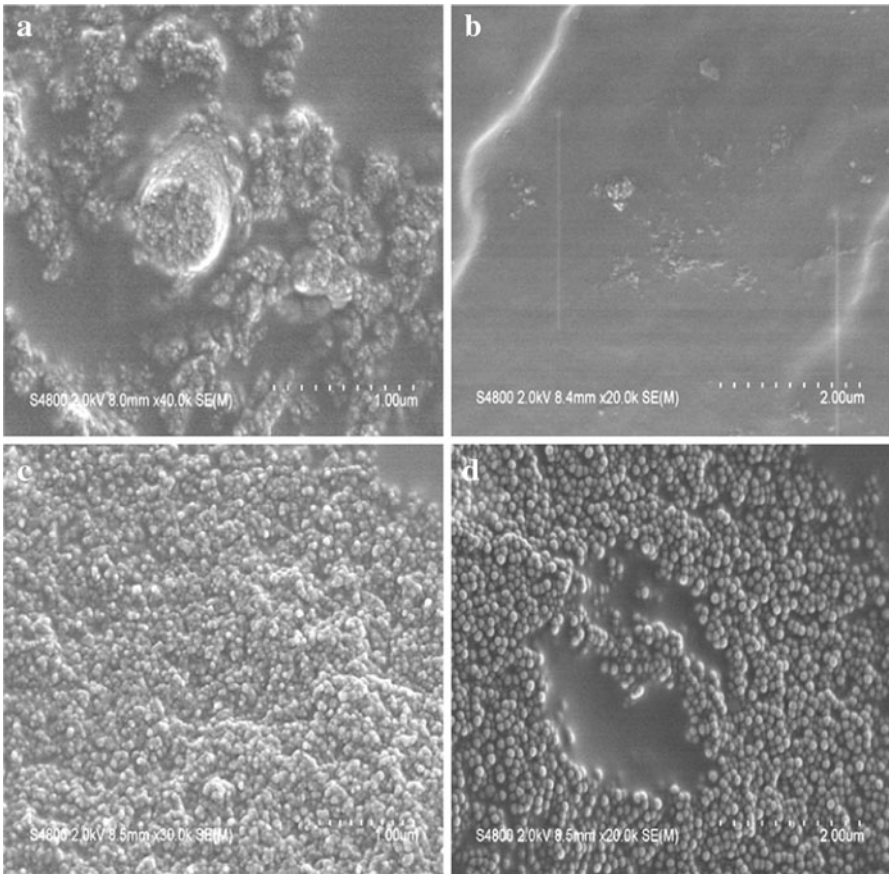

Fig. 2 SEM diagrams of the WUPU/silica nanocomposite films: **a** WUPU-R-301, **b** WUPU-R900, **c** WUPU-W75, **d** WUPU-MEMO

the individual silica nanoparticles with sizes about 95 nm were homogeneously dispersed in WUPU matrix (Figs. 1d, and 2d). So the MEMO surface modification prevented the formation of silica aggregates and increased the interactions between the silica particle and WUPU matrix.

Mechanical properties of the WUPU/silica nanocomposite films

The viscoelastic properties of the WUPU/silica nanocomposites were evaluated by dynamic mechanical analysis (DMA) to obtain the information of the glass transition temperature (T_g) and the crosslink density of the films. It was reported that T_g of a polymer nanocomposites can increase, no change or even decrease, depending on the interfacial interactions between the nanoparticles surface and the polymer matrix. If the particle surface is attractive or compatible with the polymer, T_g will increase; if it is repulsive or dewetting, T_g will decrease [26, 29]. Figure 3 displays DMA loss tangent (tanδ) as a function of temperature for WUPU/silica

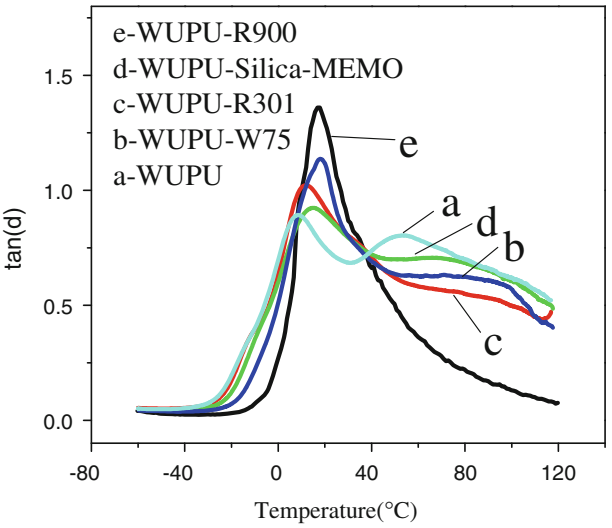

Fig. 3 Isochronal ($f = 1$HZ) temperature dependence of tanδ for WUPU/silica nanocomposite films

nanocomposite films. The pure WUPU film showed a damping peak around 9.2 °C with a small shoulder around 52.8 °C, respectively, corresponding to the T_g of soft and hard segment domains. A bit high T_g of soft segments and such a narrower difference between T_g-S and T_g-H, indicating that the pure WUPU film had limited phase separated morphology between soft and hard segments, which was most likely due to the constrained motion of the polymer chains by the formation of cross-linked WUPU networks. The nanocomposite films with R900 showed a single tanδ peak (16.9 °C), which implies the inhibition of micro-phase separation between the hard and soft segments of WUPU by the incorporation of R900. This is probably due to strong interaction between the hard segments of WUPU and silica, such that the main hard segments are bound by the silica and cross-links, leading to the overall suppression of hard segments chain relaxation motion. The R900 is an acid silica sol with cationic particles stabilized by chloride. So this strong interaction between the hard segments of PU and silica probably results from the ionic interactions between the COO^- ions hard segments of WPU and cationic silica particles. For the nanocomposite films with R301, W75, and Silica-MEMO showed the obvious broadening of the T_g-S and T_g-H peak and shifted to the high temperature, suggesting a certain interfacial interactions could exist between silica nanoparticles and WUPU molecules. For R301 and W75, this interaction may result from the hydrogen-bonding interactions between the silanol groups of silica and urethane groups of WUPU chain in the HS domains and ether groups of WUPU chain in the SS domains. But for the Silica-MEMO, this interaction may results from covalent-bonding interactions between the WUPU chain and the Silica-MEMO. For the Silica-MEMO containing more methacrylate groups on its surface is expected to participate in the photopolymerization with the methacrylate group of termini of WUPU. In a cross-linked structure, a rubbery state modulus relates

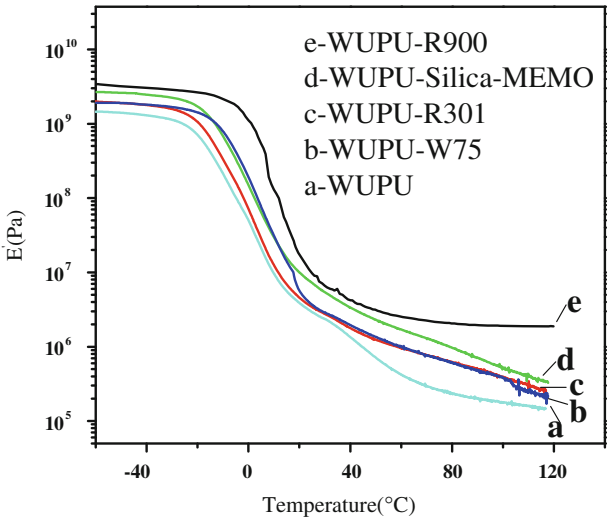

Fig. 4 Storage modulus E' in dependence on temperature for WUPU/silica nanocomposite films

directly to the network cross-link density. The cross-link density of the films was calculated with the following equation [30]: $E' = 3\ v_e\ RT$, Where v_e is the number of moles of elastically effective chains per cubic centimeter of the film. The data for the nanocomposite films is shown in Fig. 4 and Table 1. It can be seen that the storage modulus for these silica nanocomposites at temperatures above T_g was higher than that of the pure WUPU film. The adsorption of polyurethane chains onto the surface of silica particles can result in a rise in the effective degree of cross-linking and the silica can act as physical cross-linker. This enhancement was more pronounced in the case of R900 nanocomposite films due to the high cross-links density arising from the strong ionic interactions between WPU and silica particles. In addition, The WUPU/R900 nanocomposite films had a higher volume fraction of "effective" silica filler due to the well-dispersed silica particles in these polymers. While the W75 showed relatively low enhancement due to the silica particles aggregation. The Silica-MEMO was well dispersed in WUPU matrix, which resulted in the high-storage modulus in compared to the W75 nanocomposite films. But the R301 nanocomposite films showed slightly higher storage modulus than that of W75 nanocomposite films. It is probably due to the relatively small dispersion size and a higher volume fraction of "effective" silica filler in R301 nanocomposite films. In addition, to examine the degree of curing of WUPU/silica nanocomposite films, we carried out swelling tests. The gel content and swell ratio of the WUPU/silica nanocomposite films data were shown in Table 1. Since a lower degree of swelling and a high-gel contents indicates better curing, it was obvious that WUPU nanocomposite films showed high-cross-linking efficiency and much less affected by the incorporation of silica nanoparticles.

Stress–strain curves for the WUPU/silica nanocomposite films are shown in Fig. 5. The corresponding mechanical properties, Young's modulus, tensile strength, and the tensile elongation of the nanocomposite films, are summarized

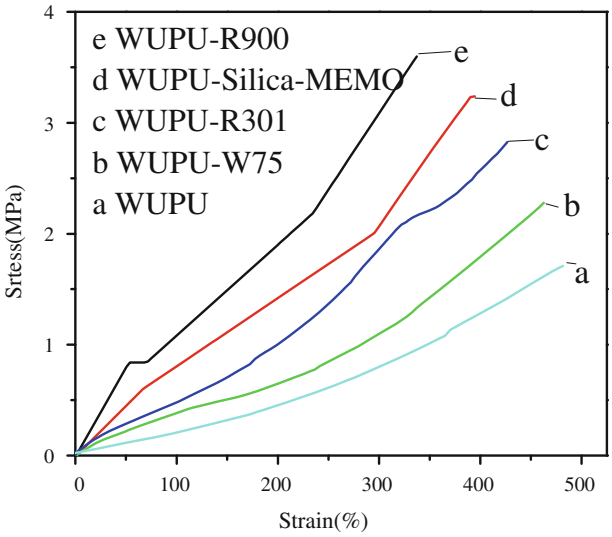

Fig. 5 Stress–strain curves for the WUPU/silica nanocomposite films

in Table 2. All the samples behaved as elastomers and their stress–strain curves were similar to theoretical ones for a Gaussian-type network, without a yield point. In general, the Young's modulus and tensile strength of the WUPU matrix was increased by the incorporation of the silica. For the nanocomposite film with R900, the tensile strength (3.62 MPa) was about 2.1 times higher than that of the pristine WUPU film (1.72 MPa). Our interpretation is that these R900 aggregates were less compact (as shown in TEM) and span a much larger volume of polymer to bring the system closer to the percolation threshold of hard material. This led to a strong reinforcement of Young's modulus and tensile strength of R900 nanocomposite films. This enhancement of mechanical properties also indicated that the stress transfered from WUPU matrix to the silica was more effective in the case of R900 nanocomposites due to the strong ionic interactions between R900 and WUPU (see Fig. 2b). However, these strong ionic interactions constrained the WUPU chain motion which resulted in the slightly low elongation of R900 nanocomposite films in compared to the pure WUPU film. In contrast, the tensile strength of WUPU nanocomposites with R301 and W75 were lower than that of the R900 nanocomposite film due to the much compact silica aggregate structure. While for the Silica-MEMO nanocomposites, due to the well dispersion of the Silica-MEMO particles and the strong covalent-bonding interaction between Silica-MEMO and WUPU, the tensile strength was higher than those of the R301 and W75 nanocomposite films. But the tensile strength of Silica-MEMO nanocomposites was still lower than that of the R900 nanocomposites. Oberdisse [31] reported that the silica aggregates were shown to have strong reinforcement at constant hard filler volume fraction and the influence of this interfacial interaction would be of second order with respect to the structural contribution.

Table 2 Mechanical properties of the WUPU/silica nanocomposite films

Sample	Elongation at break (%)	Tensile strength (MPa)	Young' modulus (GPa)	Hardness (Shore A)
WUPU	483	1.72	0.34	65
WUPU-R900	340	3.62	1.82	89
WUPU-silica-MEMO	393	3.23	1.12	85
WUPU-R301	428	2.80	0.78	82
WUPU-W75	462	2.29	0.63	79

The Shore A hardness of the WUPU films, which reflects polymer stiffness, is significantly increased by the incorporation of the silica nanoparticles (see Table 2). The hardness of a polymer film can be related to the mechanical properties of a polymer film such as Young's modulus. From this study, it can be observed that for a high value of Young's modulus, a high Shore A hardness value is also observed. The high hardness of the WUPU nanocomposites should make them especially attractive for water-based UV-curing scratch-resistant coatings.

Optical properties of WUPU/silica nanocomposite films

The obtained WUPU/silica nanocomposite films were all transparent with various silica at 10 wt% content. Since the sizes of silica nanoparticles or aggregates are smaller than the wavelength of visible light and the refractive indices of the WUPU matrix and silica nanofiller are close. So their optical differences cannot be distinguished with naked eyes. Figure 6 shows the transmittance of WUPU/silica nanocomposite films in the wavelength range of 200–800 nm. The transmittance of WUPU/silica nanocomposite films in the visible light region decreased due to the incorporation of silica nanoparticles in WUPU matrix. The transmittance at 633 nm significantly decreases from 58.20 of the pure WUPU to 23.10% of the W75 nanocomposites and to 29.52% of the R301 nanocomposites. In contrast, the transparency of R900 and Silica-MEMO nanocomposite films was slightly reduced due to the well dispersion of silica nanoparticels in WUPU matrix as shown in Fig. 2. So the WUPU/silica nanocomposite films are essentially transparent and can be used for clearcoat in coating industry.

Thermal stability of WUPU/silica nanocomposite films

Figure 7 shows a typical TGA plot of WUPU/silica nanocomposite films. The thermograms revealed two stage degradation processes; the onset of first stage of thermal degradation is in the temperature range of 245–290 °C. The second stage degradation starts at 358–426 °C. There were no significant variations in the thermal stability of WUPU and its silica nanocomposite films at initial decomposition temperatures. This stage is attributed to the thermal degradation of urethane linkages. But at higher temperatures, improved thermal stability of the WUPU nanocomposite films is evident, which can be probably due to the thermal insulation effect of nanosilica (Scheme 1).

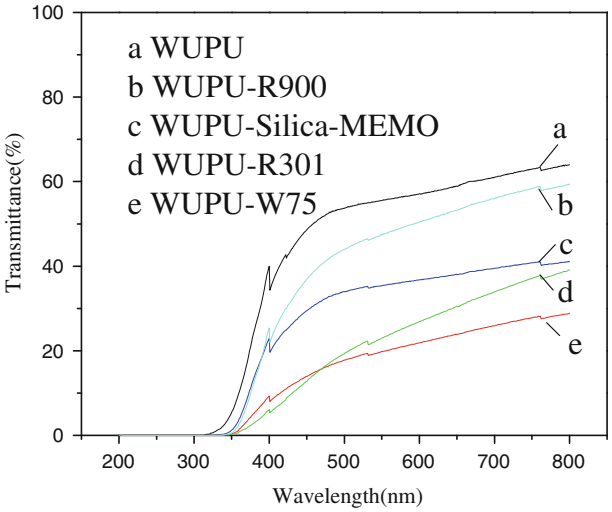

Fig. 6 Transmittance variation of the WUPU/silica nanocomposite films (ca. 0.5 mm thickness) with various silica

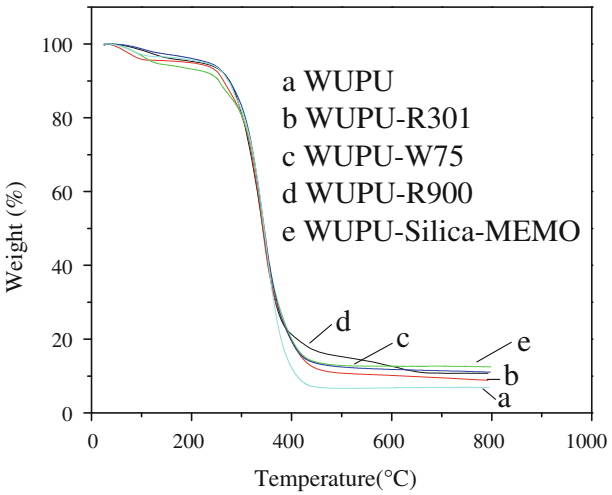

Fig. 7 TGA curves of WUPU/silica nanocomposite films

Conclusions

The WUPU/silica nanocomposites were prepared using various silica by phase-inversion emulsification method. The effect of silica surface chemistry and particles size on the microstructure and properties of WUPU/silica nanocomposite films were evaluated. TEM examinations of nanostructured films indicated that the organic

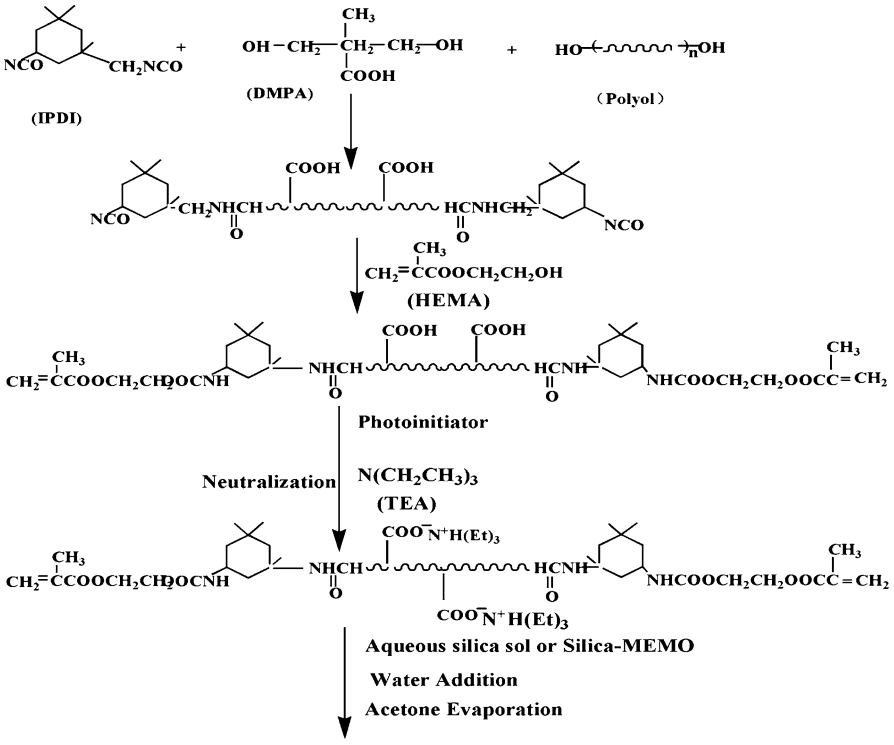

Scheme 1 Elementary steps for the synthesis of the WUPU/silica nanocomposites

modified nanosilica (Silica-MEMO) was well dispersed in the WUPU matrix, while acid (R900), and alkaline silica (R301) formed much less compact and densely aggregated structure. DMA analysis demonstrated that the WUPU/silica nanocomposite films had a broadening of the tanδ peak and shifted to higher temperature. The WUPU/silica nanocomposite films displayed enhanced storage modulus, Shore A hardness, tensile strength without sacrificing high elongation at break compared to that of the pure WUPU film. The transparency of WUPU/silica nanocomposite films strongly depend on the state of silica nanoparticles dispersion. The WUPU nanocomposite films with R900 or Silica-MEMO showed higher transparency than that of R301 or W75 nanocomposite films. The resulting nanocomposite films are possibly interesting for the generation of waterborne UV-curable WUPU nanocomposite coatings.

Acknowledgments We are grateful for the support of National Nature Science Foundation (No. 51003041) of China and the Self-determined Research Program of Jiangnan University (JUSRP30905).

References

1. Madbouly SA, Otaigbe JU (2009) Recent advances in synthesis, characterization and rheological properties of polyurethanes and POSS/polyurethane nanocomposites dispersions and films. Prog Polym Sci 34:1283–1332
2. Kro′l P (2007) Synthesis methods chemical structures and phase structures of linear polyurethanes. Properties and applications of linear polyurethanes in polyurethane elastomers, copolymers and ionomers. Prog Mater Sci 52:915–1015
3. Yang CH, Liao WT (2006) Hybrids of colloidal silica and waterborne polyurethane. J Colloid Interf Sci 302:123–132
4. Kim BS, Park SH, Kim BK (2006) Nanosilica-reinforced UV-cured polyurethane dispersion. Colloid Polym Sci 284:1067–1072
5. Sowa C, Riedla B, Blancheta P (2010) Kinetic studies of UV-waterborne nanocomposite formulations with nanoalumina and nanosilica. Prog Org Coat 67:188–194
6. Jeona HT, Janga MK, Kima BK, Kimb KH (2007) Synthesis and characterizations of waterborne polyurethane–silica hybrids using sol–gel process. Colloids Surf A 302:559–567
7. Yeh JM, Yao CT, Hsieh CF, Yang HC, Wu CP (2008) Preparation and properties of amino-terminated anionic waterborne-polyurethane–silica hybrid materials through a sol–gel process in the absence of an external catalyst. Eur Polym J 44:2777–2783
8. Sowa C, Riedla B, Blancheta P (2011) UV-waterborne polyurethane-acrylate nanocomposite coatings containing alumina and silica nanoparticles for wood: mechanical, optical, and thermal properties assessment. J Coat Technol Res 8:211–221
9. Lee HT, Lin LH (2006) Waterborne polyurethane/clay nanocomposites: novel effects of the clay and its interlayer ions on the morphology and physical and electrical properties. Macromolecules 39: 6133–6141
10. Rahman MM, Kim HD, Lee WK (2008) Preparation and characterization of waterborne polyurethane/clay nanocomposite: effect on water vapor permeability. J Appl Polym Sci 110:3697–3705
11. Deng X, Liu F, Luo Y, Chen Y, Jia D (2007) Preparation, structure and properties of comb-branched waterborne polyurethane/OMMT nanocomposites. Prog Org Coat 60:11–16
12. Lee HT, Wang JJ, Liu HJ (2006) Effects of ionic interactions between clay and waterborne polyurethanes on the structure and physical properties of their nanocomposite dispersions. J Polym Sci 44:5801–5807
13. Won J, Kim H (2005) Comparison of the properties of waterborne polyurethane/multiwalled carbon nanotube and acid-treated multiwalled carbon nanotube composites prepared by in situ polymerization. J Polym Sci 43:3973–3985
14. Kuan HC, Ma CCM, Chang WP, Yuen SM, Wu HH, Lee TM (2005) Synthesis, thermal, mechanical and rheological properties of multiwall carbon nanotube/waterborne polyurethane nanocomposite. Compos Sci Technol 65:1703–1710
15. Cai DY, Song M (2007) Water-based polyurethane filled with multi-walled carbon nanotubes prepared by a colloidal-physics method. Macromol Chem Phys 208:1183–1189
16. Chang PR, Chen FA, Dufresne YA, Huang J (2009) Effects of starch nanocrystal-graft-polycaprolactone on mechanical properties of waterborne polyurethane-based nanocomposites. J Appl Polym Sci 111:619–627
17. Chen G, Wei M, Chen J, Huang J, Dufresne A, Chang PR (2008) Simultaneous reinforcing and toughening: new nanocomposites of waterborne polyurethane filled with low loading level of starch nanocrystals. Polymer 49:1860–1870
18. Nanda AK, Wicks DA, Madbouly SA, Otaigbe JU (2006) Nanostructured polyurethane/POSS hybrid aqueous dispersions prepared by homogeneous solution polymerization. Macromolecules 39: 7037–7043
19. Turri S, Levi M (2005) Structure, dynamic properties and surface behavior of nanostructured ionomeric polyurethanes from reactive polyhedral oligomeric silsesquioxanes. Macromolecules 38: 5569–5574
20. Awad S, Chen HM, Chen GD, Gu XH, Lee JL, Hady EEA, Jean YC (2011) Free volumes, glass transitions, and cross-links in zinc oxide/waterborne polyurethane nanocomposites. Macromolecules 44:29–38
21. Goda H, Frank CW (2001) Fluorescence studies of the hybrid composite of segmented polyurethane and silica. Chem Mater 13:2783–2787

22. Zhang SW, Liu R, Jiang JQ, Yang C, Chen MQ, Liu XY (2011) Facile synthesis of waterborne UV-curable polyurethane/silica nanocomposites and morphology, physical properties of its nano-structured films. Prog Org Coat 70:1–8
23. Zhang SW, Zhou SX, Weng YM, Wu LM (2005) Synthesis of SiO_2/polystyrene nanocomposite particles via miniemulsion polymerization. Langmuir 21:2124–2128
24. Akcora P, Liu HJ, Kumar SK et al (2009) Anisotropic self-assembly of spherical polymer-grafted nanoparticles. Nature Mater 8:354–359
25. Korley LTJ, Liff SM, Kumar N, McKinley GH, Hammond PT (2006) Preferential association of segment blocks in polyurethane nanocomposites. Macromolecules 39:7030–7036
26. Bansal A, Yang H, Li CZ et al (2005) Quantitative equivalence between polymer nanocomposites and thin polymer films. Nat Mater 4:693–698
27. Akcora P, Kumar SK, Sakai VG, Li Y, Benicewicz BC, Schadler LS (2010) Segmental dynamics in PMMA-Grafted nanoparticle composites. Macromolecules 43:8275–8281
28. Geiser V, Leterrier Y, Manson JE (2010) Rheological behavior of concentrated hyperbranched polymer/silica nanocomposite suspensions. Macromolecules 43:7705–7712
29. Bansal A, Yang H, Li C, Benicewicz BC, Kumar SK, Schadler LS (2006) Controlling the thermo-mechanical properties of polymer nanocomposites by tailoring the polymer–particle interface. J Polym Sci 44:2944–2950
30. Wicks ZW, Jones FN, Pappas SP (1999) Organic Coatings. Wiley, New York
31. Oberdisse J (2006) Aggregation of colloidal nanoparticles in polymer matrices. Soft Matter 2:29–36